High-Frequency Radar Observations of Ocean Surface Currents

Jeffrey D. Paduan[1] and Libe Washburn[2]

[1]Department of Oceanography, Naval Postgraduate School, Monterey, California 93943; email: paduan@nps.edu

[2]Department of Geography and Earth Research Institute, University of California, Santa Barbara, California 93106; email: washburn@eri.ucsb.edu

Annu. Rev. Mar. Sci. 2013. 5:115–36

First published online as a Review in Advance on September 4, 2012

The *Annual Review of Marine Science* is online at marine.annualreviews.org

This article's doi: 10.1146/annurev-marine-121211-172315

Keywords

HF radar, ocean remote sensing, search and rescue, sea echo

Abstract

This article reviews the discovery, development, and use of high-frequency (HF) radio wave backscatter in oceanography. HF radars, as the instruments are commonly called, remotely measure ocean surface currents by exploiting a Bragg resonant backscatter phenomenon. Electromagnetic waves in the HF band (3–30 MHz) have wavelengths that are commensurate with wind-driven gravity waves on the ocean surface; the ocean waves whose wavelengths are exactly half as long as those of the broadcast radio waves are responsible for the resonant backscatter. Networks of HF radar systems are capable of mapping surface currents hourly out to ranges approaching 200 km with a horizontal resolution of a few kilometers. Such information has many uses, including search and rescue support and oil-spill mitigation in real time and larval population connectivity assessment when viewed over many years. Today, HF radar networks form the backbone of many ocean observing systems, and the data are assimilated into ocean circulation models.

1. INTRODUCTION

The ocean surface is driven directly by wind and buoyancy forcing, and hence circulation processes tend to be strongest and most variable in this layer. The surface is also where many human activities occur, including transportation, fishing, warfare, waste disposal, and recreation. Measurement systems that can map ocean surface currents over wide areas with high spatial and temporal resolution are critical for understanding air-sea interaction, coastal circulation, tidal flows, and related ecological processes. If the current measurements are available in real time, then the systems can support search and rescue operations, help direct toxic-spill mitigation activities, and warn of hazards such as approaching tsunamis. Remote sensing systems using high-frequency (HF) radio signals backscattered from the ocean surface are capable of mapping surface currents with the necessary spatial and temporal resolution.

HF radars rely on Doppler backscatter observations in the HF portion of the electromagnetic spectrum in the frequency range f of 3 MHz to 50 MHz, the upper end of which is in the very-high-frequency (VHF) band (Paduan & Graber 1997). These fluctuations correspond to wavelengths $\lambda = c/f$ of 100 m to 6 m, where c is the speed of light (3.00×10^8 m s^{-1}). They lie between the familiar frequencies employed for AM radio (~1 MHz) and FM radio (~100 MHz), and therefore the instruments are sometimes referred to as HF radio systems to avoid confusion with the more common microwave radars, which have wavelengths of ~1 cm.

Crombie (1955) first observed that the peak energy of HF radio waves reflected from the sea surface occupies a narrow frequency range, leading him to conclude that this resulted from backscatter from trains of surface gravity waves whose wavelengths equaled half the transmitted radio wavelength—an example of a phenomenon known as Bragg scattering. Crombie also found that the Doppler frequency shift of the backscattered radio waves agreed well with that predicted from the known phase speed of surface gravity waves traveling radially toward or away from the radio transmitter. Subsequent studies further clarified the relationship between radio signals backscattered from the sea surface and characteristics of the surface gravity wave fields producing the backscatter (e.g., Barrick 1971a,b, 1972; Barrick et al. 1974; Hasselmann 1971). Barrick (1978) reviewed the theoretical development of HF radar scattering from the sea surface and its application to physical oceanography. These early studies provided the theoretical basis for using backscattered radio signals to measure ocean surface currents.

In an important early study, Stewart & Joy (1974) observed that there are often small frequency differences between the observed Doppler shift of the backscattered radio waves and the Doppler shift predicted from surface gravity waves moving over still water. Using radar-tracked surface drogues to directly measure ocean currents, they showed that the observed differences resulted from near-surface ocean currents and that current speeds toward or away from the radars could be estimated. These findings are the basis for the mapping of surface currents by modern oceanographic HF radars.

Since the observations of Stewart & Joy (1974), many validation studies comparing HF radar–derived surface currents with in situ observations have contributed to the growing acceptance and use of HF radar for measuring surface currents (e.g., Chapman & Graber 1997; Emery et al. 2004; Essen & Gürgel 2000; Essen et al. 1989; Hammond et al. 1987; Hodgins 1994; Holbrook & Frisch 1981; Lawrence & Smith 1986; Matthews et al. 1988; Ohlmann et al. 2007; Paduan & Rosenfeld 1996; Paduan et al. 2006; Schott et al. 1985; Shay et al. 1998b, 2002). These studies found reasonable agreement between currents measured by HF radars and currents measured by other approaches, such as current meters and drifters. Graber et al. (1997) reviewed the differences and errors in HF radar–measured surface currents along with the limitations imposed by the validation methods.

While HF radar theory developed, so did the necessary hardware for measuring ocean surface currents. Crombie's (1955) system could not unambiguously identify the arrival directions of backscattered signals. Barrick et al. (1977) and Leise (1984) described a mobile, compact system comprising three antenna elements that could determine the range and arrival directions. Today, HF radar systems for mapping surface currents may be classified into two types, beam-forming and direction-finding, based on the method used to determine arrival directions.

Beam-forming radars use a linear array of antenna elements that are steered by adjusting the amplitudes and phases of received signals (e.g., Teague et al. 1997). An early beam-forming radar used extensively for mapping surface currents was the ocean surface current radar (OSCR) (Prandle & Ryder 1985, Shay et al. 2002). More recently, the Wellen radar (WERA) was developed to study surface currents and surface gravity waves (Gürgel et al. 1999a) using, most often, beam-forming configurations with up to 16 antenna elements. Note that because of the long wavelengths, it is not practical to steer HF radars mechanically, as is commonly done with microwave radars.

To achieve smaller footprints, direction-finding configurations are used. These radars compare the phases and amplitudes of radio signals received by closely spaced antenna elements coupled with various direction-finding inversion algorithms. The most common direction-finding radar is the CODAR SeaSonde (Barrick 2008), a system that evolved from earlier NOAA radars (Barrick et al. 1977). The SeaSonde employs a compact receive antenna with two crossed-loop elements and one monopole element to determine arrival directions. Further details on the characteristics and operating constraints of beam-forming and direction-finding radars are given by Barrick et al. (1977), Gürgel et al. (1999b), and Teague et al. (1997).

2. MEASURING SURFACE CURRENTS WITH HIGH-FREQUENCY RADAR

A single HF radar measures the component of surface current v_r directed radially toward or away from the radar over many small sectors surrounding the radar. The sectors typically extend over a few degrees of azimuth and a few kilometers in range from the radar. Estimation of v_r over a sector of the sea surface requires an HF radar to measure the Doppler frequency shift corresponding to v_r along with the distance from the radar to the sector. The total surface current vectors at points on the sea surface are computed from v_r measurements from two or more radars with overlapping coverage.

The Doppler frequency shift corresponding to v_r is obtained from the spectrum of backscattered signals from a sector of ocean surface, typically measured over a period of several minutes. **Figure 1** shows an example spectrum. Its main features are two strong, narrow peaks (hereafter referred to as Bragg peaks) due to backscattering from surface waves with wavelengths equaling half the radar wavelength. Other smaller, broader peaks, the so-called second-order parts of the spectrum, result from surface gravity waves spread over a range of wavelengths.

The Bragg peaks occur near the frequencies $\pm f_b$, where

$$f_b = g/\pi\lambda. \quad (1)$$

In this equation, f_b is the Doppler shift above or below the transmit frequency (shown at zero frequency in **Figure 1**), g is the acceleration of gravity, and λ is the radar wavelength. The equation assumes that the backscattering results from ocean waves traveling at deepwater phase speeds $(gL/2\pi)^{1/2}$, where the wavelength L is less than half the water depth. For a radar frequency of 12 MHz, $L \approx 12$ m and deepwater behavior occurs at depths exceeding ~6 m. Therefore, in

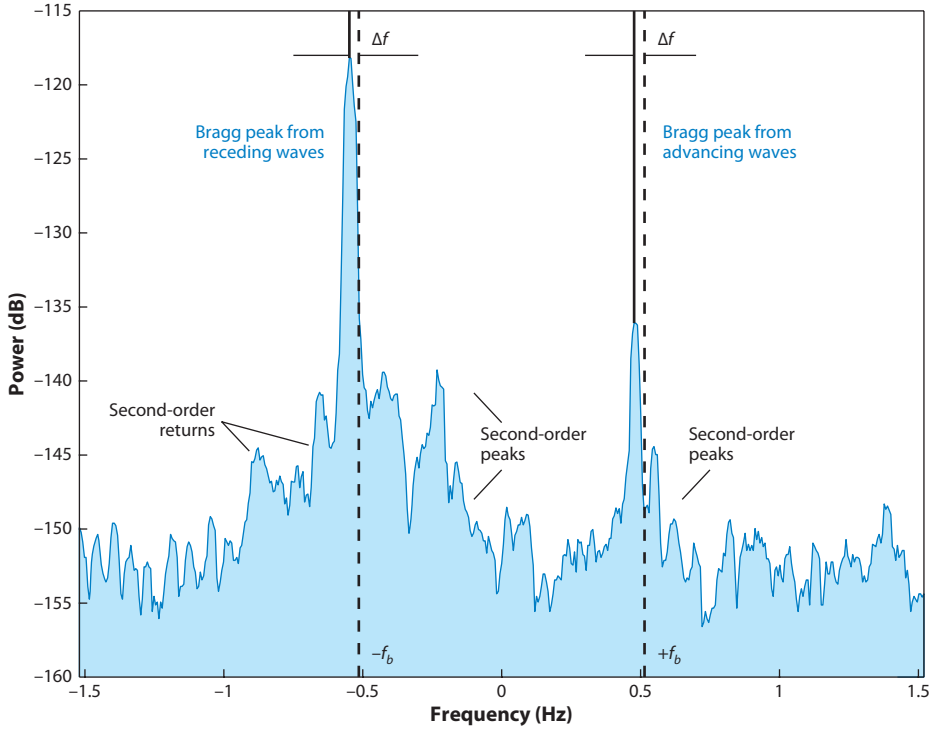

Figure 1

Doppler spectrum from an ocean surface current radar (OSCR) system operating at 25.4 MHz. The dashed lines indicate the positive and negative first-order peak frequencies predicted based on the deepwater phase speeds of the Bragg-resonant surface waves approaching and receding from the receiver, respectively. An additional frequency offset (Δf) is detectable, resulting from the surface current velocity component in the direction of the receiver, which in this OSCR example is flowing away from the receiver. Adapted from Graber et al. (1997).

most coastal areas where surface currents are measured by HF radar, Equation 1 is applicable. A nonzero v_r causes a further Doppler shift Δf because the moving ocean waves producing $\pm f_b$ have an additional velocity component due to underlying surface currents. By measuring Δf, one can determine the surface current component v_r using the well-known Doppler formula

$$\Delta f = 2v_r/\lambda. \quad (2)$$

The widths of the Bragg peaks and the method for determining Δf corresponding to a given sector depend on the type of radar.

The spectrum shown in **Figure 1** is from a beam-forming OSCR system, and the Bragg peaks are very narrow because the electronics and software "steer" the radar to obtain v_r from a single sector of the sea surface (Graber et al. 1997). In contrast, spectra from direction-finding radars have wider Bragg peaks because they result from many values of v_r spread over a ring of sectors centered on the radar (hereafter referred to as a range ring). The SeaSonde collects three spectra from signals received on three colocated antenna elements; two elements are cross-loops with directional responses to incoming signals and one element is an omnidirectional monopole (Barrick 2008). The values of v_r for individual sectors around a range ring correspond to Δf frequency shifts in the Bragg peaks. Azimuth angles to the sectors around the range ring are

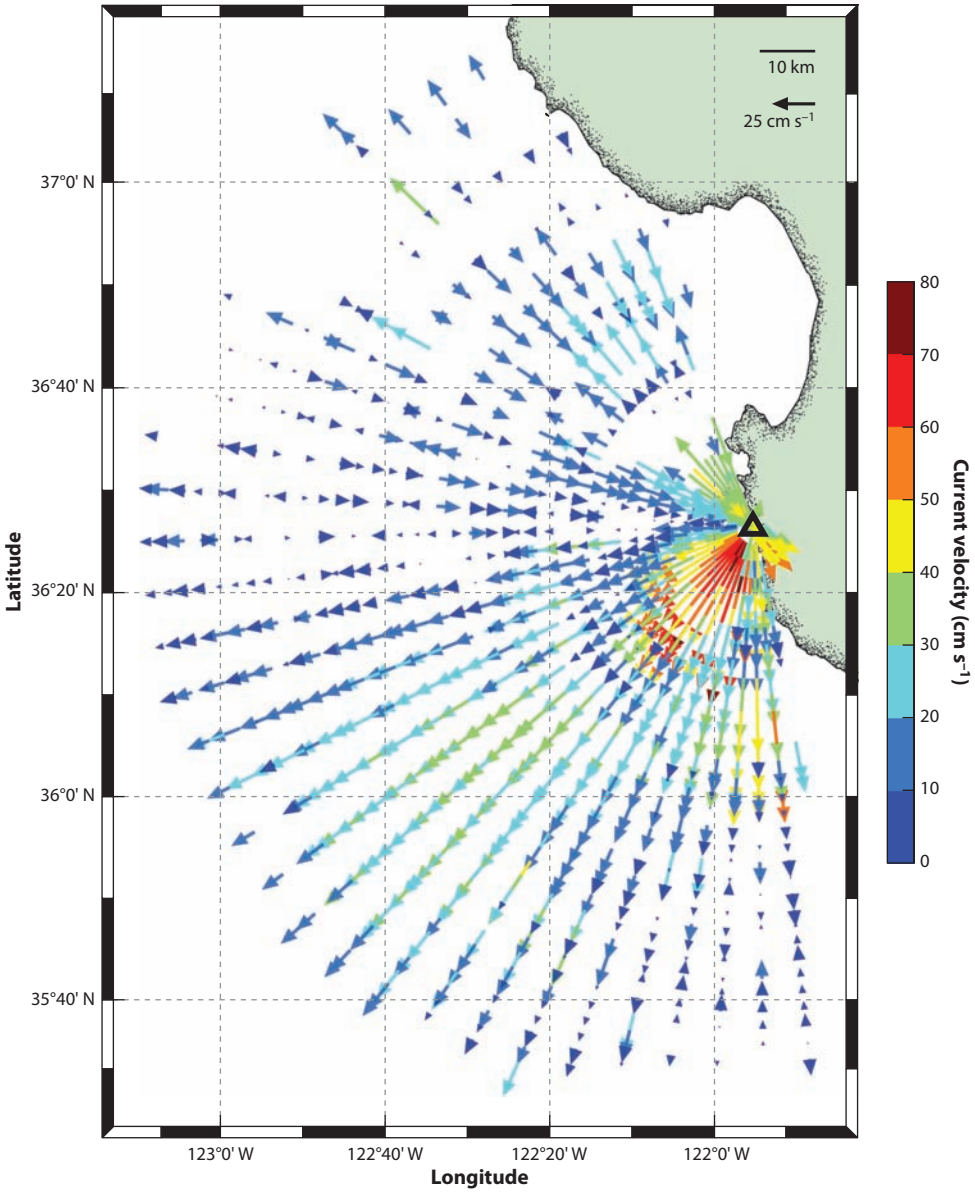

Figure 2

Hourly radial current velocity component map from a CODAR SeaSonde radar operating near 12 MHz at the Granite Canyon location south of Monterey Bay, California, at 01:00 GMT on February 2, 2011.

obtained using estimation techniques such as multiple signal classification (MUSIC) (Schmidt 1986) or least squares (Lipa & Barrick 1983). For both beam-forming and direction-finding radars, v_r is mapped over many range rings around the radars. **Figure 2** shows an example of a v_r pattern around a SeaSonde radar near Monterey Bay, California. The range over which v_r can be obtained depends upon the radar power, sea state, and background radio noise levels, but in general it is inversely proportional to frequency.

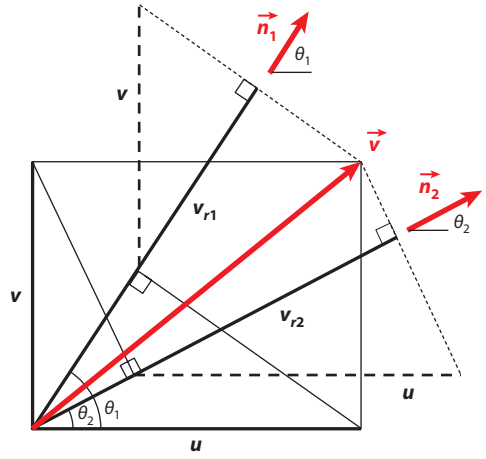

Figure 3

Geometry of the radial current component observations from two radar sites (v_{r1} and v_{r2}) and their relationships to the east–west and north–south velocity components (u and v, respectively).

Following Gürgel (1994), the east–west (u) and north–south (v) components of the surface current vector may be found by solving

$$u \cos\theta_1 + v \sin\theta_1 = v_{r1}, \tag{3}$$

$$u \cos\theta_2 + v \sin\theta_2 = v_{r2}. \tag{4}$$

Here, v_{r1} and v_{r2} are radial currents from the two radar sites and angles θ_1 and θ_2 are measured counterclockwise from the east (**Figure 3**). As the directions of v_r from the two sites become more parallel, radar measurement errors in v_r are amplified through the geometric dilution of precision (GDOP), which was described for this situation by Chapman et al. (1997). At the limit when the v_r currents from the two sites are parallel, it is impossible to resolve the component of surface velocity orthogonal to the directions of v_r. If data are available from only two sites, then the surface current vectors near the line connecting the sites—the so-called baseline—are typically not displayed owing to their large errors.

If a point on the sea surface lies in the coverage area of $n = 3$ or more radars, then u and v can be obtained from a linear least-squares solution to the system of equations expressed in matrix form as

$$\begin{vmatrix} \cos\theta_1 & \sin\theta_1 \\ \vdots & \vdots \\ \cos\theta_n & \sin\theta_n \end{vmatrix} \begin{vmatrix} u \\ v \end{vmatrix} = \begin{vmatrix} v_{r1} \\ \vdots \\ v_{rn} \end{vmatrix} \tag{5}$$

or as

$$A \cdot a = b. \tag{6}$$

The spatial resolution of the mapped u and v depends on the chosen grid spacing d_g and any additional averaging to increase n in Equation 5. Typical values of d_g are 0.5 km for the highest transmit frequencies (~45 MHz), 2–3 km for intermediate frequencies (25–12 MHz), and 5–7 km for lower frequencies (~5 MHz). Especially with direction-finding radars, which often produce coverage gaps in v_r, n is increased by incorporating values of v_r within a specified distance d_r from grid points to form the matrices in Equation 5. Typical values of d_r are 1–5 km, with higher

transmit frequencies corresponding to smaller d_r; however, because angular separation increases with range, it may be necessary to have a range-dependent $d_r > 5$ km at the greatest ranges.

3. APPLICATIONS OF OCEAN SURFACE CURRENT MAPPING DATA

This section presents the results of a number of studies employing HF radar data in order to illustrate the range of applications of this technology. The list is far from complete and is not intended to comprehensively represent the vast number of studies incorporating surface current data derived from HF radar.

The spatial and temporal resolution of HF radars makes them well suited for observing coastal ocean currents. Presently, there are no other observational approaches that can map coastal surface currents on comparable spatial and temporal scales. Altimeter satellites, for example, can map surface currents, but only on much larger scales farther offshore and under the assumption that the observed flows are in geostrophic balance, and their temporal resolution is limited by the repeat cycle of satellite passes over the ocean, which can be on the order of several days. HF radars, in contrast, map the total surface currents (geostrophic plus Ekman) on hourly timescales to offshore distances on the order of 100 km; the extent of alongshore mapping is limited only by the number of radar systems with overlapping coverage.

3.1. Wind-Driven Currents

HF radars have been used to derive surface currents in many studies of wind-driven coastal currents (Kim et al. 2009a, Kohut et al. 2006, Kosro 2005, Paduan & Rosenfeld 1996). For example, Kosro (2005) examined subtidal currents in shelf waters off the Oregon coast during the upwelling season (April–September 2001) using observations from an array of five HF radars. A sequence of surface current maps from the radars combined with wind stress time series clearly illustrated links between coastal currents and winds. The coastal currents rapidly responded to changing nearshore wind patterns, accelerating southward as upwelling wind stress increased and then slowing or reversing as wind stress relaxed or became downwelling-favorable. The Ekman response of the upper ocean has been shown in a number of studies offshore of Oregon (Zelenke 2005), China (Zhao et al. 2011), Korea (Son et al. 2007), and Japan (Yoshikawa & Masuda 2009, Yoshikawa et al. 2007), among others.

Extended deployments of HF radars allow the determination of long-term circulation patterns and the identification of transient current responses from infrequent forcing events such as hurricanes. For example, Paduan & Rosenfeld (1996) calculated monthly averages to determine the low-frequency evolution of surface current patterns in Monterey Bay. They found that a strong equatorward-flowing current jet crossed the mouth of the bay in summer and fall; this jet formed the offshore limb of a cyclonic eddy that filled most of the bay. In late fall and winter, the flow in the bay becomes more irregular and the large persistent eddy is usually absent. Kohut et al. (2006) examined the inner-shelf response to Tropical Storm Floyd as it moved along the New Jersey coastline in 1999, in the process passing directly over a coastal ocean observatory. Two HF radars operated continuously during the storm and observed currents that rapidly changed from flowing equatorward along the coast before the storm's arrival, to offshore at the storm's peak, and then to poleward following the storm. The changing phase and amplitude of the inertial response to storm winds were also quantified.

3.2. Buoyancy-Driven Currents

Buoyant coastal currents from river discharge and the cross-shelf transport of freshwater have been observed with HF radars in a range of coastal settings (Castelao et al. 2008, Chant et al.

2008, Kudela et al. 2010). An array of standard-range (12–13 MHz) and long-range (∼5 MHz) HF radars were employed in a large interdisciplinary study to examine the ecosystem dynamics associated with the outflow of the Columbia River plume (Hickey et al. 2010). Kudela et al. (2010) showed a map derived from the HF radars of equatorward alongshore currents and an anticyclonic eddy on the edge of the freshwater bulge of the Columbia River plume. Bulge formation is often an important dynamical component of the mixing of river plumes into the coastal ocean. Chant et al. (2008) used HF radar on timescales of several days to observe the evolution of the freshwater bulge of the Hudson River plume and its surface velocity field under the influence of tidal mixing and variable wind stress.

Using an array of four long-range and two higher-resolution (25 MHz) HF radars, Castelao et al. (2008) observed the offshore transport of freshwater from the Hudson River over the New Jersey shelf. Time series of surface transport were significantly correlated with salinity increases on the shelf, and the authors concluded that much of the transport resulted from an offshore current jet rather than Ekman transport. The radars provided observational evidence for the existence of the jet, and this was corroborated by surface current trajectories determined using drifting buoys.

Most buoyant plumes in the coastal ocean originate from freshwater inputs of river discharge. In some cases, however, they result from temperature differences between plume waters and the coastal ocean. Melton et al. (2009) and Washburn et al. (2011) employed surface current maps from an array of five HF radars to describe the structure and propagation of warm buoyant coastal currents following wind relaxations along the central California coast. The surface current maps quantified the propagation speeds, velocity structure, and cross-shore spatial scales of the plumes as they move poleward along the coast.

3.3. Eddies in the Coastal Ocean

A number of observational studies of eddies in the coastal ocean have relied on HF radars to quantify important aspects of their kinematics, such as size, vorticity $\zeta = \partial v/\partial x - \partial u/\partial y$, and duration. Based on HF radar observations off the southwest coast of Oahu, Chavanne et al. (2010b) observed the evolution of a small (∼15 km), rapidly rotating (ζ on the order of the Coriolis parameter f) anticyclone that persisted for 9 days. High-resolution HF radar observations allowed them to estimate the dominant terms in the momentum and vorticity budgets. They also evaluated a number of instability mechanisms that could have accounted for the rapid decay and expansion of the anticyclone over several days.

Rapidly evolving cyclonic eddies on comparable spatial scales were observed with HF radar in the Florida Current by Graber & Limouzy-Paris (1997), Limouzy-Paris et al. (1997), and Shay et al. (2000). The eddies propagated at ∼25 km day^{-1} along the inshore edge of the Florida Current and had azimuthal velocities of ∼0.5 m s^{-1}. The ζ of the eddies was very large, in the range of $5f$ to $7f$, as reported by Parks et al. (2009). Shay et al. (1998a) observed the interaction between one of these eddies and a wavelike feature in the near-inertial frequency band. The ζ of the eddy was large enough to shift the frequency of the wavelike feature by a few percent of f, as described by Kunze (1985). During these Florida Current observations, the flow speeds measured by the HF radars were corroborated by observations from acoustic Doppler current profilers (ADCPs) in the radar coverage area.

Bassin et al. (2005) used HF radar to observe rapidly evolving anticyclonic eddies with diameters of 4–15 km and ζ of $-0.4f$ to $-0.8f$ near the shore in the Southern California Bight. Unlike those in the Florida Current, these eddies did not propagate and typically lasted 2 days, with a few lasting up to 6 days. These eddies also transported nutrients to the inner shelf, suggesting that they are an important mechanism for delivering subsidies to coastal ecosystems such as kelp forests.

Although eddies are a dominant source of surface current variability in the coastal ocean, few studies on their occurrence over large areas of the coastal ocean have been conducted. The primary limitations have been the small coverage areas of many HF radar networks and the lack of methods for detecting eddies automatically. The increasing number of HF radars for mapping surface currents is overcoming the first limitation (e.g., Int. Telecommun. Union Radio Commun. Sect. 2010, Paduan et al. 2004), and algorithm development is overcoming the second. Automated algorithms based on the geometry of surface current velocity vectors (Kim 2010, Nencioli et al. 2010) allow the detection of eddies over large areas and long time periods. For example, Kim (2010) used an automated detection algorithm to quantify kinematic parameters of eddies off the coast of San Diego during 2003–2005.

3.4. Tidal Processes

The mapping of surface tidal currents was one of the earliest applications of HF radar observations (e.g., Broche et al. 1986, Prandle 1987) and remains important. Time series analysis techniques, such as the harmonic analysis routines within the T_Tide package (Pawlowicz et al. 2002), can be applied to individual observation grid locations to separate the tidal constituents from other fluctuations. The length of the data record determines the number of constituents that can be independently evaluated. Importantly, the harmonic analysis is relatively insensitive to noise or data gaps. Tidal patterns have been revealed or validated for many locations around the world using HF radar observations, including offshore of Great Britain (Prandle 1991), in Monterey Bay (Paduan & Cook 1997, Petruncio 1993, Petruncio et al. 1998, Rosenfeld et al. 2009), offshore of New Jersey (Kohut et al. 2004), in the northern Adriatic Sea (Chavanne et al. 2007), and downstream of Hawaii (Chavanne et al. 2010a).

The use of HF radar observations of tidal currents in model validation and data assimilation is discussed below. Spatial patterns in observed tidal currents can reveal hidden processes, particularly where complex bathymetry creates strong internal tides. Petruncio (1993) revealed surprising patterns of M_2 tidal currents in Monterey Bay. At those frequencies, the surface flow is out of the bay during times when the sea level is rising (**Figure 4**). Those observations led to a number of subsequent studies of the internal tidal currents that propagate toward shore along the axis of the Monterey Submarine Canyon (e.g., Carter et al. 2005, Kunze et al. 2002, Petruncio et al. 1998). The behavior of the semidiurnal internal tidal currents in Monterey Bay differs fundamentally from that of the diurnal currents at the surface, represented by the K_1 fluctuations. In the latter case, surface currents are affected by sea breeze wind forcing that extends only a few meters into the water column (Paduan & Cook 1997, Paduan & Rosenfeld 1996). Long records (greater than 1 year) are required to separate this wind effect from the diurnal tidal forcing (Rosenfeld et al. 2009).

3.5. Mapping of Coastal Currents over Large Spatial Areas and Long Timescales

The expanding coverage of national HF radar networks (e.g., Paduan et al. 2004) is enabling the observation of dynamical processes in the coastal ocean on an unprecedented range of spatial and temporal scales. A recent study by Kim et al. (2011) demonstrated the potential of using many HF radars to map surface currents across very large spatial scales—in this case, the entire US west coast—and over multiple years. This study, based on 2 years of data (2007–2008), revealed a wide variety of coastal ocean phenomena, including wavelike signals propagating at various speeds along the coast, more than 2,000 eddies on scales of 10–60 km, and a variety of wind-driven current processes distributed along the coast. Two types of wavelike signals were observed, one with phase

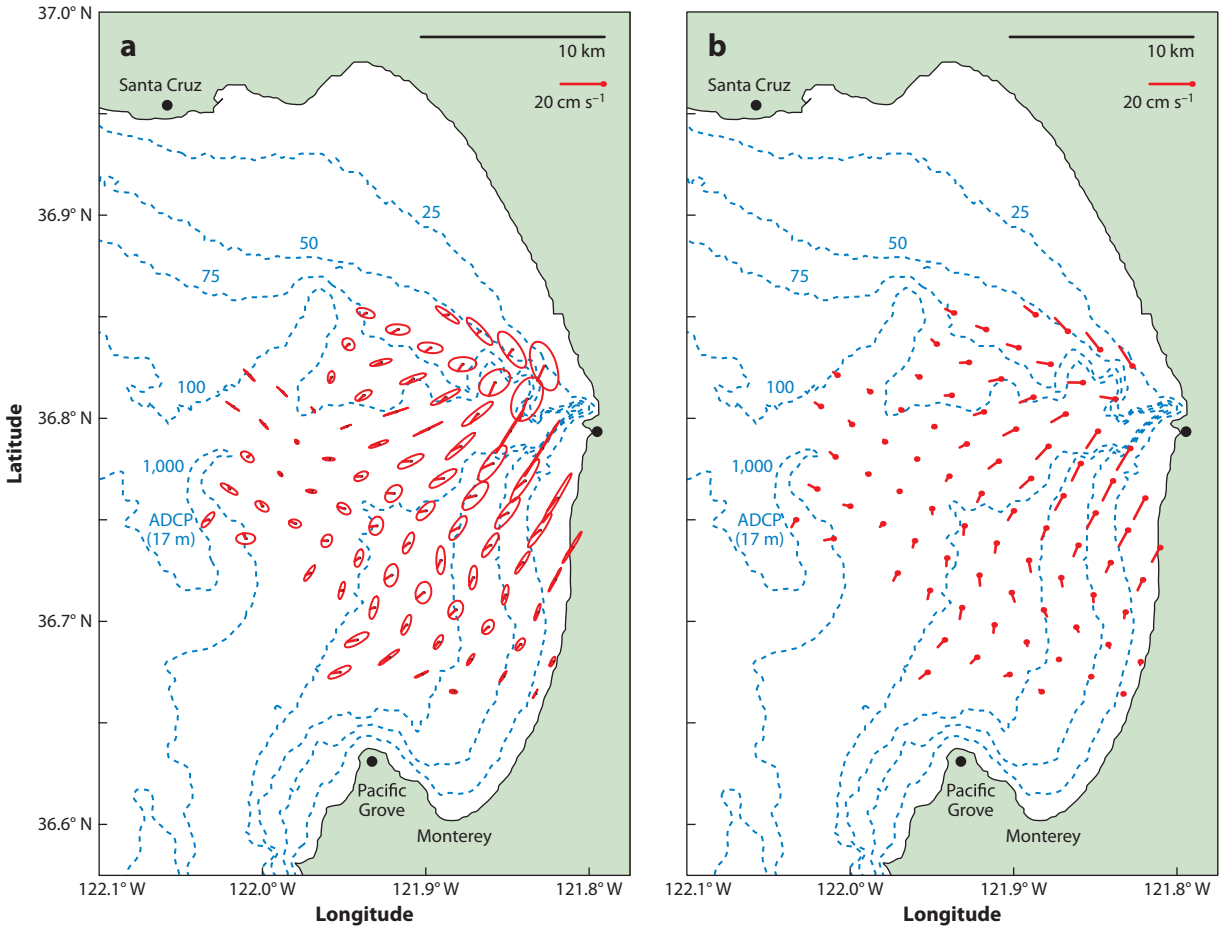

Figure 4

(*a*) M_2 tidal current ellipses (*red*) based on high-frequency radar from September 1992, shown with lines extending out from the center to represent the direction toward which the current flows and its speed at the time of high-M_2 sea level. (*b*) Current flow 3 h prior to high-M_2 sea level, shown with the flow directed away from the red dots, which mark the centers of the radar bins. Depth contours (*blue*) are in meters. Abbreviation: ADCP, acoustic Doppler current profiler. Adapted from Petruncio et al. (1998).

speeds on the order of 10 km day^{-1} and a second with speeds on the order of 100–300 km day^{-1}. An interesting observation was that the slower-propagating signals were found mainly in southern California, suggesting that they were scattered by coastline irregularities such as the bend at Point Conception. The faster-propagating signals, in contrast, were identifiable over longer stretches of the coastline.

3.6. Ocean Circulation Modeling: Model Validation

The wide spatial coverage provided by HF radar networks is useful in validating ocean circulation models in both real-time and retrospective modes. In the former, the validation tends to be qualitative, but it can be particularly useful in operational settings in which output from a number of competing models is available. Such was the case during the Deepwater Horizon oil spill in the Gulf of Mexico. Although HF radar coverage was not available for much of the area of

concern during that prolonged spill, hazardous material responders compared model results daily against surface velocity observations for the area of overlap offshore of Mississippi in order to determine which of the several models appeared to be most accurately simulating the circulation (G. Watabayashi, personal communication). Similar qualitative validation of individual models using surface current observations has appeared in a number of publications, including several studies of the circulation around Monterey Bay (Chao et al. 2009; Shulman et al. 2002, 2007), the circulation in the Santa Barbara Channel (Dong et al. 2009), and the circulation off the Oregon coast (Kurapov et al. 2005).

The power of surface current mapping data is the spatial structure, or lack thereof, that it can elucidate. Circulation models can reasonably be expected to exhibit the same patterns, especially from a statistical point of view. Comparison of spatial empirical orthogonal function (EOF) patterns from HF radar observations and from (similarly sampled) model results is one way to provide statistical model validation. This approach was taken for Monterey Bay by Paduan & Shulman (2004), for the Oregon continental shelf by Erofeeva et al. (2003), and for the region off the mouth of the Columbia River by Liu et al. (2009). As the surface current mapping data become more extensive and persist over longer durations, the power of the EOF technique can be applied to larger domains, such as the central California region described by Kaplan et al. (2009). EOF pattern information can also form the basis for improved short-term trajectory forecasts if sufficiently long training sets are available, as shown by Frolov et al. (2012). The ultimate utility of surface current mapping data is illustrated by the analyses of Kim et al. (2011), which revealed dynamical processes that suggest deficiencies in the way most numerical models treat the very-near-surface layer. HF radar–derived wavenumber spectra, for example, were shown to exhibit a k^{-2} roll-off at high wavenumbers, in agreement with two-dimensional, quasi-geostrophic submesoscale theory and some modern circulation models (e.g., Capet et al. 2008).

The near-surface mixing processes are also made more subtle through the effects of Stokes drift, which is captured by HF radar observations but not by truly Eulerian current meters (Mao & Heron 2008). Ardhuin et al. (2009) investigated this effect in detail by comparing HF radar observations and wave model results. They showed that the wind-coherent portion of the surface current varies in magnitude from 1% to 2% of the wind speed and in direction from 10° to 40° to the right of the wind, depending on the wave conditions.

A very specific and critical process that HF radar observations can validate is that of the tidal current patterns at the ocean surface. As discussed above, tidal currents are one of the more robust observations made by HF radar systems. Harmonic analysis can determine the spatially varying orientations, amplitudes, and phases of the tidal currents, even in the presence of significant noise and with missing data blocks. The agreement of model and observed tidal current patterns is an important expectation of a validated circulation model, particularly in regions for which tidal currents dominate the flow or show particularly complex spatial variations. Rosenfeld et al. (2009), for example, concluded that their tidally forced numerical model was not producing the proper internal tidal currents because it could not reproduce the observed pattern of surface currents. Using an alternate model formulation in the same Monterey Bay domain, Wang et al. (2009) obtained slightly better results, but, as the authors stated, "there is much room for improvement in terms of magnitude and spatial pattern." Wang et al. (2009) also found their tidal solutions to be sensitive to their model's stratification, which is consistent with the expectation that internal tidal currents are dominant in that region. In other regions—such as offshore of Great Britain (Prandle 1991), in the northwest Adriatic Sea (Chavanne et al. 2007), downstream of Hawaii (Chavanne et al. 2010a), and along the Oregon coast (J.J. Osborne, A.L. Kurapov, G.D. Egbert & P.M. Kosro, manuscript in review)—HF radar–derived tidal ellipses confirm modeled tidal currents.

3.7. Ocean Circulation Modeling: Data Assimilation

Beyond model validation, the ultimate use of surface current mapping data is expected to be as a systematic input to operational, three-dimensional ocean circulation models. Data-assimilating ocean models have the advantage of maintaining a dynamically consistent interpolation framework and the ability, given reliable atmospheric forcing predictions, to forecast future ocean conditions. For applications limited to transport at the ocean surface, such as search and rescue, oil-spill mitigation, and buoyant larvae advection, direct use of observed surface currents combined with statistical models (e.g., Frolov et al. 2012, O'Donnell et al. 2012, Zelenke 2005) can suffice. The benefits of and need for data-assimilating numerical models become clear when dealing with subsurface processes or very long forecast times (more than a few days). The hypothesis being tested in a number of situations is the assumption that the assimilation of ocean surface current maps from HF radar systems into three-dimensional circulation models will improve the model results at the surface as well as for some finite distance below the surface and beyond the observation footprint (Oke et al. 2002).

The seemingly obvious assumption that the inclusion of observed surface information will improve model results obscures the many choices to be made when defining a particular modeling system. This section briefly summarizes the data-assimilation testing that has taken place in recent years using surface current mapping data. Both the availability of wide-area surface current mapping data and the use of velocity as an assimilation data source are recent phenomena; there is no long-running program of velocity assimilation into which new HF radar–based observations can be easily inserted. Numerical weather prediction and the parallel efforts in the ocean look to integral constraints, such as density profiles, where available. Scalar boundary conditions, such as sea surface temperature observations from satellites, are also commonly used. The assimilation of velocity information from surface currents or winds, however, is not common. Wide-area coverage of these data has only recently been available, and the covariance and cross-covariance error statistics needed for most assimilation methods are not well known.

A number of modeling studies using a variety of methods and error models have been conducted to assess the impact of surface current assimilation. Although there is not yet a consensus as to the optimal methodology, the results have been encouraging. Surface current mapping data can improve model simulations and forecasts at the surface and within a finite portion of the upper ocean (e.g., **Figure 5**) (Breivik & Saetra 2001, Gopalakrishnan 2008, Oke et al. 2002, Paduan & Shulman 2004, Tinis et al. 1996, Yu et al. 2012). Assimilation methods incorporating surface current observations fall into broad categories, including optimal interpolation or nudging methods (e.g., Breivik & Saetra 2001, Gopalakrishnan 2008, Oke et al. 2002, Tinis et al. 1996, Wilkin et al. 2005), truncated or ensemble Kalman filtering methods (e.g., Paduan & Shulman 2004, Shulman & Paduan 2009, Xu 2010), and three- or four-dimensional variational methods (e.g., Hoteit et al. 2009, Wilkin et al. 2011, Yu et al. 2012, Zhang et al. 2010). Assimilation techniques have been applied to the u and v velocity components of the mapped vector velocities. Shulman & Paduan (2009), however, showed that improved results can be obtained by directly assimilating radial current component data from individual radar sites, presumably owing to the increased spatial coverage available when radial currents are used.

Although the full error covariance matrices between surface current observations and the three-dimensional model state variables are not available, various approaches to estimating these statistical functions have been used. In some cases, the error covariances have been assumed to be linearly proportional to the data covariances. Paduan & Shulman (2004) and Shulman & Paduan (2009) used observed two-dimensional monthly velocity covariance functions to provide a seasonally varying error model for Monterey Bay. The projection of surface information downward

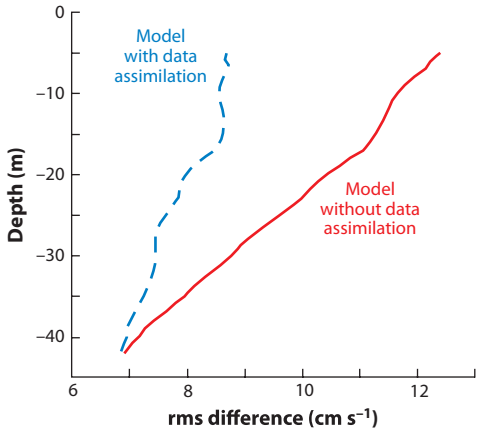

Figure 5

Root mean square (rms) difference between modeled and observed velocities on the west Florida shelf with and without the assimilation of surface current data. Adapted from Barth et al. (2008).

in the models represents an additional challenge. In the Monterey Bay case, very thin boundary layer formulations were used to absorb the velocity corrections, and—as argued by Paduan & Shulman (2004)—correction divergences act to extend the influence downward through a type of Ekman pumping correction. This approach was also used earlier in Monterey Bay by Lewis et al. (1998) and in the Strait of Georgia by Tinis et al. (1996). These early studies used a nudging timescale to force model surface currents toward the observed surface currents.

All of these surface-only approaches can be thought of as a form of correction to unknown or poorly known wind forcing. They are not, however, only a correction for overly smoothed wind fields. Shulman & Paduan (2009) used wind forcing on scales commensurate with the surface current observations (3 km) but found that the model was still improved by the assimilation of the surface current data.

Other approaches to the vertical projection problem have also been taken. In the continental shelf setting offshore of New Jersey, Wilkin et al. (2005) used vertical correlation functions observed at mooring sites to develop transfer functions between surface and water column velocities. The predetermined projection functions were then applied to the surface current assimilation problem using continuous nudging or intermittent melding techniques. As an aside, a body of work related to projecting HF radar–derived surface current observations throughout the water column was suggested by Shen & Evans (2001) for continental shelf settings. Their approach assumes frictional boundary layer dynamics at the top and bottom of the column to couple observed surface currents and surface shear (via wind stress) to orthogonal basis functions covering the entire water column. They demonstrated the method using OSCR-derived currents and wind observations near Cape Hatteras. Cosoli (2007) furthered this work using data from the Adriatic Sea offshore of Venice.

A common approach in many assimilation studies has been to create an ensemble of model runs and use the model's three-dimensional covariance functions between surface current and other variables as a proxy for the actual data covariances. This approach has the benefit of allowing for consistent assimilation schemes among all input variables and eliminates the need for ad hoc boundary layer assumptions. It does, however, depend upon the model and its forcing fields being representative of the real-world conditions. Oke et al. (2002) helped to pioneer this approach

for the Oregon continental shelf following the model-based assessments of Scott et al. (2000). This approach was also used on the west Florida shelf by Barth et al. (2008) and over intermediate depths offshore of Norway by Xu (2010). A recent adaptation of these methods by Oke et al. (2009) for the region inshore of the East Australia Current showed significant model improvement for surface velocity, as might be expected, and for temperature and salinity at 205 m depth as well as sea surface elevation. Interestingly, the improvements at depth and in sea surface elevation were shown to be comparable to a single repeated glider line through the model domain.

Recently, increasing computer power has enabled four-dimensional variational approaches to be tested. In these studies, the error covariances are constantly updated within the model over assimilation windows of, typically, 3 days (e.g., Wilkin et al. 2011, Yu et al. 2012, Zhang et al. 2010), although Hoteit et al. (2009) were able to stretch the assimilation window to be as wide as 10 days. The power of these techniques is well illustrated by the work of Hoteit et al. (2009) offshore of San Diego and Yu et al. (2012) offshore of Oregon. The techniques in these two studies rely on linearized adjoint models that back-project the MIT or ROMS (Regional Ocean Modeling System) models, respectively. The assimilation process adjusts forcing fields and initial boundary conditions to make the forward model results match the observed surface current maps as closely as possible. In this way, detailed information about the sensitivity of the modeled fields to the surface current information can be obtained. For the coastal ocean setting in southern California studied by Hoteit et al. (2009), it was clearly demonstrated that by far the most important parameter with respect to the sensitivity to surface current observations was the surface wind stress (**Figure 6**). This result comes full circle and is consistent with the earliest assimilation approaches that assumed that surface current observations are a proxy for incompletely observed wind stress (e.g., Lewis et al. 1998).

Finally, as described above for model validation, data-assimilation techniques specific to tidal currents are an important subset of assimilation studies. Shulman & Paduan (2009) compared the assimilation of tidally resolving surface currents against the assimilation of low-pass-filtered surface currents and found no difference in the low-pass-filtered results for their Ekman layer assimilation method in Monterey Bay. Other locations and techniques have yielded better results, however. Erofeeva et al. (2003) obtained marked improvement in tidal model results assimilating surface current data for their barotropically dominated location on the Oregon shelf. Kurapov et al. (2003) used a related generalized inverse model in the same region to investigate the M_2 internal tide; in this case, baroclinic tidal observations were used to create boundary conditions that more accurately represented the dominant externally generated M_2 signal. Zaron et al. (2009), working with observations downstream of Hawaii, produced a variational data-assimilation model to investigate the conversion of barotropic-to-baroclinic M_2 tidal energy. Although these results are speculative, they also showed that the amplitudes of the tidal residuals from the data-assimilating model matched the expected amplitude of tidal-mesoscale interactions.

3.8. Marine Ecology

Surface current mapping using HF radars has found wide application in studies of marine ecology in the coastal ocean. For example, as part of a study of eddy dynamics and fish assemblages in the Florida Strait, Graber & Limouzy-Paris (1997) and Limouzy-Paris et al. (1997) found that small eddies spun off from the Florida Current were important for dispersing reef fish larvae and transporting them to nearshore settlement sites. In another study of larval transport, Bjorkstedt & Roughgarden (1997) used data from a single HF radar site near Point Sur, California, to estimate onshore currents as they responded to cycles of upwelling-favorable winds and wind relaxations. A comparison of estimates of the (one-dimensional) divergence of onshore currents with the abundance of larval fish and barnacle larvae along a cross-shore transect revealed that

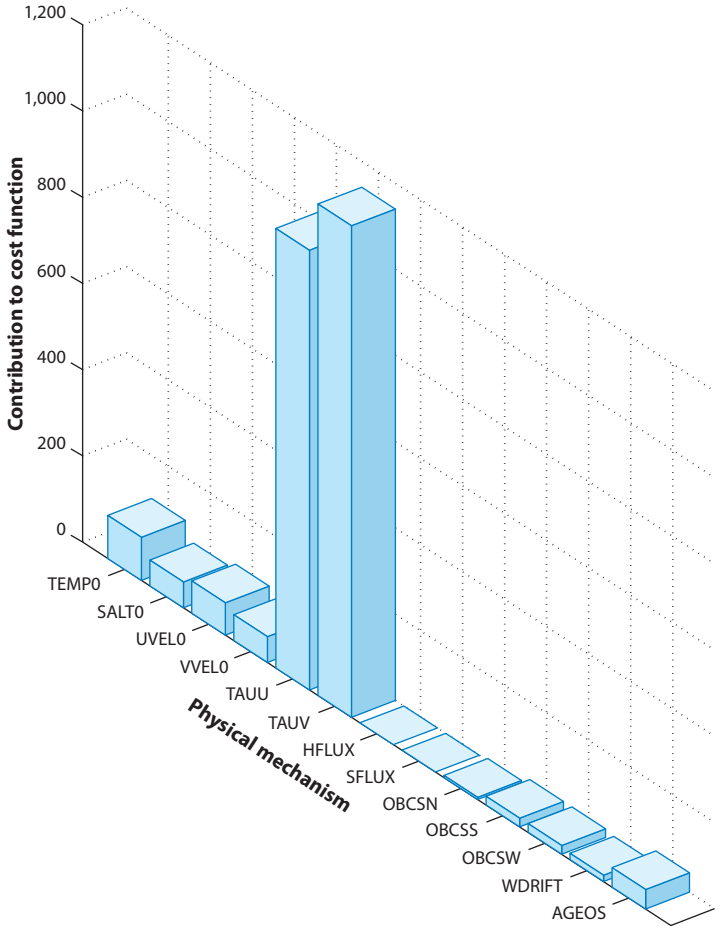

Figure 6

Individual cost function contributions for control terms after 22 optimization iterations in Hoteit et al.'s (2009) study testing a four-dimensional model of the ocean circulation offshore of San Diego with respect to surface current observations. TAUU and TAUV represent the dominant wind stress components (other physical mechanism definitions are given in Hoteit et al. 2009). Adapted from Hoteit et al. (2009).

larvae accumulated in (apparently) convergent fronts. Nishimoto & Washburn (2002) observed large aggregations of larval reef fish in the center of a cyclonic eddy that persisted for several weeks in the Santa Barbara Channel. In a second period in the same region, when another eddy appeared that was more variable and exhibited closed streamlines less consistently, large fish aggregations were not found. The evolving surface current fields of the eddies were mapped by HF radar and then used to direct shipboard trawl sampling for larval fishes in real time.

Time series of surface current maps from HF radar have proven useful in a range of Lagrangian studies of particle dispersion, larval transport, and the connectivity between larval source and settlement regions (Emery et al. 2006, Helbig & Pepin 2002, Ullman et al. 2006, Zelenke et al. 2009). To assess the connectivity among marine protected areas (MPAs) along the south-central California coast, Zelenke et al. (2009) computed reverse trajectories, each lasting 40 days, over 1 year between potential larval source regions and destinations within established MPAs. The continuous operation of the large HF radar network in this region allowed the results of thousands

of trajectories to be incorporated into connectivity matrices within the network of MPAs. Kim et al. (2009b) used forward trajectories computed from HF radar–derived surface currents to estimate shoreline exposure to fecal indicator bacteria discharged from multiple sources in southern California and northern Mexico. Using a statistical approach called receiver characteristic operating analysis, they found reasonable agreement between measured patterns of bacteria from shoreline stations and trajectories connecting the discharge points and the shoreline.

Another ecological application with policy implications is Emery et al.'s (2006) study examining the likelihood that the settlement of larval and juvenile bocaccio (*Sebastes paucispinis*) on oil production platforms reduced the settlement of these fishes on natural reefs near the shore. By reconstructing larval trajectories, they concluded that larvae settling on the platforms likely would have been advected far from shore in the absence of the platforms, and therefore it is unlikely that the platforms reduced settlement on natural reefs.

Helbig & Pepin (2002) investigated evolving spatial patterns of fish eggs in Conception Bay, Canada, based on HF radar surface current observations and concurrent shipboard ADCP and egg surveys. An ocean circulation model was used to simulate egg transport over 4 days separating the egg surveys. An important conclusion was that simulating small-scale variability in currents, particularly the divergence of horizontal currents, was critical for predicting the advection and dispersion of fish eggs.

Surface current maps have also proven useful in understanding the spatial structure and evolution of phytoplankton blooms, including harmful algal blooms in coastal waters. The anticyclonic current patterns revealed by HF radar in freshwater bulges offshore of the Columbia and Hudson Rivers led to the retention of nutrient-laden water masses, with consequent rapid growth of phytoplankton blooms (Chant et al. 2008, Hickey et al. 2010, Kudela et al. 2010). In the case of the Hudson River, nutrient retention by the anticyclonic bulge currents led to low oxygen levels following rapid phytoplankton bloom formation (Chant et al. 2008). In contrast, retention in the Columbia River bulge led to similar rapid bloom formation, but with overall positive ecosystem effects that supported higher trophic levels (Kudela et al. 2010). Similar retention of nutrients and phytoplankton within a cyclonic eddy observed by HF radar, coupled with strong upwelling-favorable winds, drove the rapid development of a harmful algal bloom throughout the Santa Barbara Channel in 2003 (Anderson et al. 2006). The highest levels of particle-associated domoic acid occurred within the cyclonic eddy. HF radar observations of current patterns with high relative vorticity led Brzezinski & Washburn (2011) to conclude that cyclonic eddy formation is related to enhanced phytoplankton primary productivity in coastal ecosystems, which has also been observed in open ocean ecosystems (e.g., Benitez-Nelson et al. 2007, McGillicuddy et al. 2007, Siegel et al. 1999).

3.9. Ocean Observing Systems

HF radars are a backbone technology for evolving coastal ocean observing systems around the world (Glenn & Schofield 2009, Heron 2009, Int. Telecommun. Union Radio Commun. Sect. 2010, Paduan et al. 2004, Shay et al. 2008). The state of California and various research programs have deployed more than 100 HF radars along the US coastline, and NOAA's Integrated Ocean Observing System (IOOS) is beginning to support operations of the national network (e.g., Seim et al. 2009, Shay et al. 2008). The radars themselves are often nested with long-range systems that provide lower spatial resolution over extensive areas and shorter-range systems that provide higher spatial resolution around busy harbors or large population centers (Glenn & Schofield 2009). An emerging application is the use of HF radars to detect tsunamis as they propagate over the continental shelf or up submarine canyons (Heron et al. 2008, Lipa et al. 2011).

Coordination between HF radar operators is strong; it is supported by IOOS in the United States and by similar efforts in Europe, Australia, and Asia. In an important development, resolution 612 of the 2012 World Radiocommunication Conference identified, for the first time, HF operating bands for oceanographic radar instruments. This ensures that HF radar systems will continue to be a growing asset to marine scientists and resource managers in the future.

DISCLOSURE STATEMENT

The authors are not aware of any affiliations, memberships, funding, or financial holdings that might be perceived as affecting the objectivity of this review.

ACKNOWLEDGMENTS

The authors would like to acknowledge support from the state of California's Coastal Ocean Currents Monitoring Program, the NOAA IOOS Program, and the National Science Foundation.

LITERATURE CITED

Anderson CR, Brzezinski M, Washburn L, Kudela R. 2006. Circulation and environmental conditions during a toxigenic *Pseudo-nitzschia australis* bloom in the Santa Barbara Channel, California. *Mar. Ecol. Prog. Ser.* 327:119–33

Ardhuin F, Marié L, Rascle N, Forget F, Roland A. 2009. Observation and estimation of Lagrangian, Stokes and Eulerian currents induced by wind and waves at the sea surface. *J. Phys. Oceanogr.* 39:2820–38

Barrick DE. 1971a. Theory of HF and VHF propagation across the rough sea, 1: the effective surface impedance for a slightly rough highly conducting medium at grazing incidence. *Radio Sci.* 6:517–26

Barrick DE. 1971b. Theory of HF and VHF propagation across the rough sea, 2: application to HF and VHF propagation above the sea. *Radio Sci.* 6:527–33

Barrick DE. 1972. First-order theory and analysis of MF/HF/VHF scatter from the sea. *IEEE Trans. Antennas Propag.* 20:2–10

Barrick DE. 1978. HF radio oceanography—a review. *Bound. Layer Meteorol.* 13:23–43

Barrick DE. 2008. 30 years of CMTC and CODAR. *Proc. IEEE OES Ninth Working Conf. Curr. Meas. Technol.*, Mar. 17–19, pp. 131–36. New York: IEEE

Barrick DE, Evans MW, Weber BL. 1977. Ocean surface currents mapped by radar. *Science* 198:138–44

Barrick DE, Headrick JM, Bogle RW, Crombie DD. 1974. Sea backscatter at HF: interpretation and utilization of the echo. *Proc. IEEE* 62:673–80

Barth A, Alvera-Azcárate A, Weisberg RH. 2008. Assimilation of high-frequency radar currents in a nested model of the West Florida Shelf. *J. Geophys. Res.* 113:C08033

Bassin CJ, Washburn L, Brzezinski M, McPhee-Shaw E. 2005. Sub-mesoscale coastal eddies observed by high frequency radar: a new mechanism for delivering nutrients to kelp forests in the Southern California Bight. *Geophys. Res. Lett.* 32:L12604

Benitez-Nelson CR, Bidigare RR, Dickey TD, Landry MR, Leonard CL, et al. 2007. Mesoscale eddies drive increased silica export in the subtropical Pacific Ocean. *Science* 316:1017–21

Bjorkstedt E, Roughgarden J. 1997. Larval transport and coastal upwelling: an application of HF radar in ecological research. *Oceanography* 10(2):64–67

Breivik Ø, Saetra Ø. 2001. Real time assimilation of HF radar currents into a coastal ocean model. *J. Mar. Sci.* 28:161–82

Broche P, Salomon JC, Demaistre JS, Devenon JL. 1986. Tidal currents in Baie de Seine: comparison of numerical modeling and high-frequency radar measurements. *Estuar. Coast. Shelf Sci.* 23:465–76

Brzezinski MA, Washburn L. 2011. Phytoplankton primary productivity in the Santa Barbara Channel: effects of wind-driven upwelling and mesoscale eddies. *J. Geophys. Res.* 116:C12013

Capet X, McWilliams JC, Molemaker MJ, Shchepetkin AF. 2008. Mesoscale to submesoscale transition in the California Current System. Part I: flow structure, eddy flux, and observational tests. *J. Phys. Oceanogr.* 38:29–43

Carter GS, Gregg MC, Lien R-C. 2005. Internal waves, solitary-like waves, and mixing on the Monterey Bay shelf. *Cont. Shelf Res.* 25:1499–520

Castelao R, Schofield O, Glenn S, Chant R, Kohut J. 2008. Cross-shelf transport of freshwater on the New Jersey shelf. *J. Geophys. Res.* 113:C07017

Chant RJ, Glenn SM, Hunter E, Kohut J, Chen RF, et al. 2008. Bulge formation of a buoyant river outflow. *J. Geophys. Res.* 113:C01017

Chao Y, Li Z, Farrara J, McWilliams JC, Bellingham J, et al. 2009. Development, implementation and evaluation of a data-assimilative ocean forecasting system off the central California coast. *Deep-Sea Res. II* 56:100–26

Chapman RD, Graber HC. 1997. Validation of HF radar measurements. *Oceanography* 10(2):76–79

Chapman RD, Shay LK, Graber HC, Edson JB, Karachintsev A, et al. 1997. On the accuracy of HF radar surface current measurements: intercomparison with ship-based sensors. *J. Geophys. Res.* 102:18737–48

Chavanne C, Flament P, Carter G, Merrifield M, Luther D, et al. 2010a. The surface expression of semidiurnal internal tides near a strong source at Hawaii. Part I: observations and numerical predictions. *J. Phys. Oceanogr.* 40:1155–79

Chavanne C, Flament P, Gürgel K-W. 2010b. Interactions between a submesoscale anticyclone and a front. *J. Phys. Oceanogr.* 40:1802–18

Chavanne C, Janekovic I, Flament P, Poulain P-M, Kuzmic M, Gürgel K-W. 2007. Tidal currents in the northwestern Adriatic: high frequency radio observations and numerical model predictions. *J. Geophys. Res.* 112:C03S21

Cosoli S. 2007. *Inference of the three-dimensional flow field in shallow water environments: application of the "Velocity Projection Technique" to the Northern Adriatic Sea*. PhD thesis. Ca' Foscari Univ., Venice. 151 pp.

Crombie DD. 1955. Doppler spectrum of sea echo at 13.56 Mc/s. *Nature* 175:681–82

Dong C, Idica EY, McWilliams JC. 2009. Circulation and multiple-scale variability in the southern California Bight. *Prog. Oceanogr.* 82:168–90

Emery BM, Washburn L, Harlan JA. 2004. Evaluating radial current measurements from CODAR high-frequency radars with moored current meters. *J. Atmos. Ocean. Technol.* 21:1259–71

Emery BM, Washburn L, Love MS, Nishimoto MM, Ohlmann JC. 2006. Do oil and gas platforms reduce the recruitment of bocaccio (*Sebastes paucispinis*) to natural habitat? An analysis based on trajectories derived from high-frequency radar. *Fish. Bull.* 104:391–400

Erofeeva SY, Egbert GD, Kosro PM. 2003. Tidal currents on the central Oregon shelf: models, data, and assimilation. *J. Geophys. Res.* 108:3148

Essen H-H, Gürgel K-W. 2000. On the accuracy of current measurements by means of HF radar. *IEEE J. Ocean. Eng.* 25:472–80

Essen H-H, Gürgel K-W, Schirmer F. 1989. Surface currents in the Norwegian Channel measured by radar in March 1985. *Tellus* 41A:162–74

Frolov S, Paduan JD, Cook MS, Bellingham J. 2012. Improved statistical prediction of surface currents based on historic HF-radar observations. *Ocean Dyn.* 62:1111–22

Glenn S, Schofield O. 2009. Growing a distributed ocean observatory: our view from the COOL room. *Oceanography* 22(2):128–45

Gopalakrishnan G. 2008. *Surface current observations using high frequency radar and its assimilation into the New York harbor observing and prediction system*. PhD thesis. Stevens Inst. Technol., Hoboken, NJ. 206 pp.

Graber HC, Haus BK, Chapman RD, Shay LK. 1997. HF radar comparisons with moored estimates of current speed and direction: expected differences and implications. *J. Geophys. Res.* 102:18749–66

Graber HC, Limouzy-Paris CB. 1997. Transport patterns of tropical reef fish larvae by spin-off eddies in the Straits of Florida. *Oceanography* 10(2):68–71

Gürgel K-W. 1994. Shipborne measurement of surface current fields by HF radar. *L'Onde Électr.* 74(5):54–59

Gürgel K-W, Antonischki G, Essen H-H, Schlick T. 1999a. Wellen Radar (WERA): a new ground-wave HF radar for ocean remote sensing. *Coast. Eng.* 37:219–34

Gürgel K-W, Essen H-H, Kingsley SP. 1999b. High-frequency radars: physical limitations and recent developments. *Coast. Eng.* 37:201–18

Hammond TM, Pattiaratchi CB, Eccles D, Osborne MJ, Nash LA, Collins MB. 1987. Ocean surface current radar (OSCR) vector measurements on the inner continental shelf. *Cont. Shelf Res.* 7:411–31

Hasselmann K. 1971. Determination of ocean wave spectra from Doppler radio return from the sea surface. *Nat. Phys. Sci.* 229:16–17

Helbig JA, Pepin P. 2002. The effects of short space and time scale current variability on the predictability of passive ichthyoplankton distributions: an analysis based on HF radar observations. *Fish. Oceanogr.* 11:175–88

Heron ML. 2009. The Australian coastal ocean radar network facility. *Proc. IEEE Can. Conf. Electr. Comput. Eng.*, St. John's, Canada, May 3–6, pp. 23–26. New York: IEEE

Heron ML, Prytz A, Heron SF, Helzel T, Schlick T, et al. 2008. Tsunami observation by coastal ocean radar. *Int. J. Remote Sens.* 29:6347–59

Hickey BM, Kudela RM, Nash JD, Bruland KW, Peterson WT, et al. 2010. River influences on shelf ecosystems: introduction and synthesis. *J. Geophys. Res.* 115:C00B17

Hodgins DO. 1994. Remote sensing of ocean surface currents with SeaSonde HF radar. *Spill Sci. Technol. Bull.* 1:109–29

Holbrook JR, Frisch AS. 1981. A comparison of near-surface CODAR and VACM measurements in the Strait of Juan de Fuca, August 1978. *J. Geophys. Res.* 86:10908–12

Hoteit I, Cornuelle B, Kim SY, Forget G, Köhl A, Terrill E. 2009. Assessing 4D-VAR for dynamical mapping of coastal high-frequency radar in San Diego. *Dyn. Atmos. Oceans* 48:175–97

Int. Telecommun. Union Radio Commun. Sect. (ITU-R). 2010. Technical and operational characteristics of oceanographic radars operating in sub-bands within the frequency range 3–50 MHz. *Recomm. ITU-R M.1874*, *04/2010*, ITU, Geneva

Kaplan DM, Halle C, Paduan J, Largier JL. 2009. Surface currents during anomalous upwelling seasons off central California. *J. Geophys. Res.* 114:C12026

Kim SY. 2010. Observations of submesoscale eddies using high-frequency radar-derived kinematic and dynamic quantities. *Cont. Shelf Res.* 30:1639–55

Kim SY, Cornuelle BD, Terrill EJ. 2009a. Anisotropic response of surface currents to the wind in a coastal region. *J. Phys. Oceanogr.* 39:1512–33

Kim SY, Terrill EJ, Cornuelle BD. 2009b. Assessing coastal plumes in a region of multiple discharges: the U.S.–Mexico border. *Environ. Sci. Technol.* 43:7450–57

Kim SY, Terrill EJ, Cornuelle BD, Jones B, Washburn L, et al. 2011. Mapping the U.S. West Coast surface circulation: a multiyear analysis of high-frequency radar observations. *J. Geophys. Res.* 116:C03011

Kohut JT, Glenn SM, Chant RJ. 2004. Seasonal current variability on the New Jersey inner shelf. *J. Geophys. Res.* 109:C07S07

Kohut JT, Glenn SM, Paduan JD. 2006. Inner-shelf response to tropical storm Floyd. *J. Geophys. Res.* 111:C09S91

Kosro PM. 2005. On the spatial structure of coastal circulation off Newport, Oregon, during spring and summer 2001 in a region of varying shelf width. *J. Geophys. Res.* 110:C10S06

Kudela RM, Horner-Devine AR, Banas NS, Hickey BM, Peterson TD, et al. 2010. Multiple trophic levels fueled by recirculation in the Columbia River plume. *Geophys. Res. Lett.* 37:L18607

Kunze E. 1985. Near-inertial wave propagation in a geostrophic shear. *J. Phys. Oceanogr.* 15:544–65

Kunze E, Rosenfeld LK, Carter GS, Gregg MC. 2002. Internal waves in Monterey Submarine Canyon. *J. Phys. Oceanogr.* 32:1890–913

Kurapov AL, Allen JS, Egbert GD, Miller RN, Kosro PM, et al. 2005. Assimilation of moored velocity data in a model of coastal wind-driven circulation off Oregon: multivariate capabilities. *J. Geophys. Res.* 110:C10S08

Kurapov AL, Egbert GD, Allen JS, Miller RN, Erofeeva SY, Kosro PM. 2003. The M_2 internal tide off Oregon: inferences from data assimilation. *J. Phys. Oceanogr.* 33:1733–57

Lawrence JD, Smith PC. 1986. Evaluation of HF ground-wave radar on the east coast of Canada. *IEEE J. Ocean. Eng.* 11:246–50

Leise JA. 1984. The analysis and digital signal processing of NOAA's surface current mapping system. *IEEE J. Ocean. Eng.* 9:106–13

Lewis JK, Shulman I, Blumberg AF. 1998. Assimilation of Doppler radar current data into numerical ocean models. *Cont. Shelf Res.* 18:541–59

Limouzy-Paris CB, Graber HC, Jones DL, Röpke A, Richards WJ. 1997. Translocation of larval coral reef fishes via submesoscale spin-off eddies from the Florida Current. *Bull. Mar. Sci.* 60:966–83

Lipa BJ, Barrick DE. 1983. Least-squares method for the extraction of surface currents from CODAR crossed-loop data: application at ARSLOE. *IEEE J. Ocean. Eng.* 8:226–53

Lipa BJ, Barrick DE, Saitoh S-I, Ishikawa Y, Awaji T, et al. 2011. Japan tsunami current flows observed by HF radars on two continents. *Remote Sens.* 3:1663–79

Liu Y, MacCready P, Hickey BM, Dever EP, Kosro PM, Banas NS. 2009. Evaluation of a coastal ocean circulation model for the Columbia River plume in summer 2004. *J. Geophys. Res.* 114:C00B04

Mao Y, Heron ML. 2008. The influence of fetch on the response of surface currents to wind studied by HF ocean surface radar. *J. Phys. Oceanogr.* 38:1107–21

Matthews JP, Simpson JH, Brown J. 1988. Remote sensing of shelf sea currents using a high-frequency ocean surface current radar system. *J. Geophys. Res.* 93:2303–10

McGillicuddy DJ Jr, Anderson LA, Bates NR, Bibby T, Buesseler KO, et al. 2007. Eddy/wind interactions stimulate extraordinary mid-ocean plankton blooms. *Science* 316:1021–26

Melton C, Washburn L, Gotschalk C. 2009. Wind relaxations and poleward flow events in a coastal upwelling system on the central California coast. *J. Geophys. Res.* 114:C11016

Nencioli F, Dong C, Dickey T, Washburn L, McWilliams JC. 2010. A vector geometry-based eddy detection algorithm and its application to a high-resolution numerical model product and high-frequency radar surface velocities in the Southern California Bight. *J. Atmos. Ocean. Technol.* 27:564–79

Nishimoto MM, Washburn L. 2002. Patterns of coastal eddy circulation and abundance of pelagic juvenile fish in the Santa Barbara Channel, California, USA. *Mar. Ecol. Prog. Ser.* 241:183–99

O'Donnell J, Ullman D, Edwards CA, Fake T, Allen A. 2012. The operational prediction of circulation and Lagrangian trajectories in the coastal ocean. *Ocean Dyn.* In press

Ohlmann C, White P, Washburn L, Terrill E, Emery BM, Otero M. 2007. Interpretation of coastal HF radar derived surface currents with high resolution drifter data. *J. Atmos. Ocean. Technol.* 24:666–80

Oke PR, Allen JS, Miller RN, Egbert GD, Kosro PM. 2002. Assimilation of surface velocity data into a primitive equation coastal ocean model. *J. Geophys. Res.* 107:3122

Oke PR, Sakov P, Shulz E. 2009. A comparison of shelf observation platforms for assimilation in an eddy-resolving ocean model. *Dyn. Atmos. Oceans* 48:121–42

Paduan JD, Cook MS. 1997. Mapping surface currents in Monterey Bay with CODAR-type HF radar. *Oceanography* 10(2):49–52

Paduan JD, Graber HC. 1997. Introduction to high frequency radar: reality and myth. *Oceanography* 10(2):36–39

Paduan JD, Kim KC, Cook MS, Chavez FP. 2006. Calibration and validation of direction-finding high frequency radar ocean surface current observations. *IEEE J. Ocean. Eng.* 31:862–75

Paduan JD, Kosro PM, Glenn SM. 2004. A national coastal ocean surface current mapping system for the United States. *Mar. Technol. Soc. J.* 38(2):102–8

Paduan JD, Rosenfeld LK. 1996. Remotely sensed surface currents in Monterey Bay from shore-based HF radar (CODAR). *J. Geophys. Res.* 101:20669–86

Paduan JD, Shulman I. 2004. HF radar data assimilation in the Monterey Bay area. *J. Geophys Res.* 109:C07S09

Parks AB, Shay LK, Johns WE, Martinez-Pedraja J, Gürgel K-W. 2009. HF radar observations in the Straits of Florida. *J. Geophys. Res.* 114:C08002

Pawlowicz R, Beardsley R, Lentz S. 2002. Classical tidal harmonic analysis including error estimates in MATLAB using T_TIDE. *Comput. Geosci.* 28:929–37

Petruncio ET. 1993. Characterization of tidal currents in Monterey Bay from remote and in-situ measurements. MS thesis. Nav. Postgrad. Sch., Monterey, CA. 113 pp.

Petruncio ET, Rosenfeld LK, Paduan JD. 1998. Observations of the internal tide in Monterey Submarine Canyon. *J. Phys. Oceanogr.* 28:1873–903

Prandle D. 1987. The fine-structure of nearshore tidal and residual circulations revealed by H.F. radar surface current measurements. *J. Phys. Oceanogr.* 17:231–45

Prandle D. 1991. A new view of near-shore dynamics based on observations from HF radar. *Prog. Oceanogr.* 27:403–38

Prandle D, Ryder DK. 1985. Measurement of surface currents in Liverpool Bay by high-frequency radar. *Nature* 315:128–31

Rosenfeld L, Shulman I, Cook M, Paduan J, Shulman L. 2009. Methodology for a regional tidal model evaluation with application to central California. *Deep-Sea Res. II* 56:199–219

Schmidt RO. 1986. Multiple emitter location and signal parameter estimation. *IEEE Trans. Antennas Propag.* 34:276–80

Schott F, Frisch AS, Leaman K, Samuels G, Foting IP. 1985. *J. Geophys. Res.* 90:9006–16

Scott RK, Allen JS, Egbert GD, Miller RN. 2000. Assimilation of surface current measurements in a coastal ocean model. *J. Phys. Oceanogr.* 30:2359–78

Seim HE, Fletcher M, Mooers CNK, Nelson JR, Weisberg RH. 2009. Towards a regional coastal ocean observing system: an initial design for the Southeast Coastal Ocean Observing Regional Association. *J. Mar. Syst.* 77:261–77

Shay LK, Cook TM, Haus BK, Martinez J, Peters H, et al. 2000. VHF radar detects oceanic submesoscale vortex along Florida coast. *Eos Trans. AGU* 81:209–13

Shay LK, Cook TM, Peters H, Mariano AJ, Weisberg R, et al. 2002. Very high-frequency radar mapping of surface currents. *IEEE J. Ocean. Eng.* 27:155–69

Shay LK, Lee TN, Williams EJ, Graber HC, Rooth CGH. 1998a. Effects of low-frequency current variability on near-inertial submesoscale vortices. *J. Geophys. Res.* 103:18691–714

Shay LK, Lentz SJ, Graber HC, Haus BK. 1998b. Current structure variations detected by high-frequency radar and vector-measuring current meters. *J. Atmos. Ocean. Technol.* 15:237–55

Shay LK, Seim H, Savidge D, Styles R, Weisberg RH. 2008. High frequency radar observing systems in SEACOOS: 2002–2007 lessons learned. *Mar. Technol. Soc. J.* 42(3):55–67

Shen CY, Evans TE. 2001. Surface-to-subsurface velocity projection for shallow water currents. *J. Geophys. Res.* 106:6973–84

Shulman I, Kindle K, Martin P, deRada S, Doyle J, et al. 2007. Modeling of upwelling/relaxation events with the Navy Coastal Ocean Model. *J. Geophys. Res.* 112:C06023

Shulman I, Paduan JD. 2009. Assimilation of HF radar-derived radials and total currents in the Monterey Bay area. *Deep-Sea Res. II* 56:149–60

Shulman I, Wu C-R, Lewis JK, Paduan JD, Rosenfeld LK, et al. 2002. High resolution modeling and data assimilation in the Monterey Bay area. *Cont. Shelf Res.* 22:1129–51

Siegel DA, McGillicuddy DJ Jr, Fields EA. 1999. Mesoscale eddies, satellite altimetry, and new production in the Sargasso Sea. *J. Geophys. Res.* 104:13359–79

Son Y-T, Lee S-H, Kim C-S, Lee JC, Lee G-H. 2007. Surface current variability in the Keum River Estuary (South Korea) during summer 2002 as observed by high-frequency radar and coastal monitoring buoy. *Cont. Shelf Res.* 27:43–63

Stewart RH, Joy JW. 1974. HF radar measurement of surface current. *Deep-Sea Res.* 21:1039–49

Teague CC, Vesecky JF, Fernandez DM. 1997. HF radar instruments past to present. *Oceanography* 10(2):40–44

Tinis SW, Hodgins DO, Fingas M. 1996. Assimilation of radar measured surface current fields into a numerical model for oil spill modeling. *Spill Sci. Technol. Bull.* 3:247–51

Ullman DS, O'Donnell J, Kohut J, Fake T, Allen A. 2006. Trajectory prediction using HF radar surface currents: Monte Carlo simulations of prediction uncertainties. *J. Geophys. Res.* 111:C12005

Wang X, Chao Y, Dong C, Farrara J, Li Z, et al. 2009. Modeling tides in Monterey Bay, California. *Deep-Sea Res. II* 56:219–31

Washburn L, Fewings MR, Melton C, Gotschalk C. 2011. The propagating response of coastal circulation due to wind relaxations along the central California coast. *J. Geophys. Res.* 116:C12028

Wilkin JL, Arango HG, Haidvogel DB, Lichtenwalner CS, Glenn SM, Hedström KS. 2005. A regional ocean modeling system for the long-term ecosystem observatory. *J. Geophys. Res.* 110:C06S91

Wilkin JL, Zhang WG, Cahill B, Chant RC. 2011. Integrating coastal models and observations for studies of ocean dynamics, observing systems and forecasting. In *Operational Oceanography in the 21st Century*, ed. A Schiller, G Brassington, pp. 487–512. Dordrecht: Springer

Xu J. 2010. *Assimilation of high frequency radar data into a shelf sea circulation model*. PhD thesis. Univ. Hamburg. 113 pp.

Yoshikawa Y, Masuda A. 2009. Seasonal variations in the speed factor and deflection angle of the wind-driven surface flow in the Tsushima Strait. *J. Geophys. Res.* 114:C12022

Yoshikawa Y, Matsuno T, Marubayashi K, Fukudome K. 2007. A surface velocity spiral observed with ADCP and HF radar in the Tsushima Strait. *J. Geophys. Res.* 112:C06022

Yu P, Kurapov AL, Egbert GD, Allen JS, Kosro PM. 2012. Variational assimilation of HF radar surface currents in a coastal ocean model off Oregon. *Ocean Model.* 49–50:86–104

Zaron ED, Chavanne C, Egbert GD, Flament P. 2009. Baroclinic tidal generation in the Kauai Channel inferred from high-frequency radio Doppler current meters. *Dyn. Atmos. Oceans* 48:93–120

Zelenke B. 2005. *An empirical statistical model relating winds and ocean surface currents: implications for short-term current forecasts*. MS thesis. Ore. State Univ., Corvallis. 94 pp.

Zelenke B, Moline M, Crawford G, Garfield N, Jones B, et al. 2009. Evaluating connectivity between marine protected areas using CODAR high-frequency radar. *Proc. OCEANS 2009 MTS/IEEE Biloxi*, Biloxi, MS, Oct. 26–29, pp. 2261–70. New York: IEEE

Zhang WG, Wilkin JL, Arango HG. 2010. Towards an integrated observation and modeling system in the New York Bight using variational methods. Part I: 4DVAR data assimilation. *Ocean Model.* 35:119–33

Zhao J, Chen X, Hu W, Chen J, Guo M. 2011. Dynamics of surface currents over Qingdao coastal waters in August 2008. *J. Geophys. Res.* 116:C10020

Annual Review of
Marine Science

Volume 5, 2013

Contents

Errata

An online log of corrections to *Annual Review of Marine Science* articles may be found at http://marine.annualreviews.org/errata.shtml